RESEARCH LETTER

blood advances

TO THE EDITOR:

Digital pathology in pediatric nodular lymphocyte-predominant Hodgkin lymphoma: correlation with treatment response

Sergej Sereda,[1,*] Ananth Shankar,[2,*] Luise Weber,[1] Alan D. Ramsay,[3] Georgina W. Hall,[4] Janis Hayward,[5] William Hamish B. Wallace,[6] Judith Landman-Parker,[7] Andreas Braeuninger,[1] Dirk Hasenclever,[8] Astrid Schneider,[9] Christine Mauz-Koerholz,[9,10,†] Dieter Koerholz,[9,†] and Stefan Gattenloehner[1,†]

[1]Department of Pathology, University Hospital Giessen and Marburg GmbH, Giessen, Germany; [2]Children and Young People's Cancer Services, University College London Hospitals NHS Foundation Trust, London, United Kingdom; [3]Department of Cellular Pathology, University College London Hospitals NHS Foundation Trust, London, United Kingdom; [4]Paediatric and Adolescent Haematology & Oncology Unit, Children's Hospital, Oxford University Hospitals NHS Foundation Trust, Oxford, United Kingdom; [5]School of Cancer Sciences, Cancer Research UK Clinical Trials Unit, University of Birmingham, Birmingham, United Kingdom; [6]Royal Hospital for Children and Young People, Edinburgh, United Kingdom; [7]Sorbonne University, Assistance Publique–Hôpitaux de Paris, Hôpital Armand-Trousseau, Paris, France; [8]Institute for Medical Informatics, Statistics and Epidemiology, University of Leipzig, Leipzig, Germany; [9]Pediatric Hematology and Oncology, University Hospital Giessen and Marburg GmbH, Giessen, Germany; and [10]Medical Faculty of the Martin-Luther-University of Halle-Wittenberg, Halle, Germany

Nodular lymphocyte-predominant Hodgkin lymphoma (NLPHL) accounts for 10% of all Hodgkin lymphoma cases.[1,2] Most patients are diagnosed in the early stages and have excellent survival rates after radio- or chemotherapy, or a combination of the two.[3,4] However, radiotherapy is not recommended for pediatric patients because of the late toxicity in aging survivors.[5] Instead, low-intensity therapy with cyclophosphamide in combination with vinblastine and prednisone (CVP) is preferred. Only patients with poor treatment response receive more intensive chemotherapy.[6] To introduce new treatment concepts based on the biology of the disease, attempts have been made to develop a histological response marker based on the morphometry and distribution of disease-defining LP cells. The classification proposed by Fan et al[7] recognizes 6 different histological patterns of NLPHL, with variant patterns C-F being considered high-risk for clinical outcomes.[8] However, the prognostic value of this classification is less clear in early-stage patients when compared with those with advanced-stage disease.[9,10] Recent research by Hartmann et al[11] has shown differences in LP cell nuclear size between early-, intermediate-, and advanced-stage NLPHL, as well as between typical and variant Fan patterns. This analysis was limited to a small number of cells per case.

We used deep-learning–based cell detection on digitized biopsy slides from early-stage pediatric patients treated within the EuroNet-PHL-LP1 trial to quantitatively assess LP-cell histology. Through whole-slide spatial analysis, we identified 6 key characteristics of LP cell spatial patterns and correlated them with treatment response to low-intensity CVP chemotherapy. In addition, we explored the relationship between treatment response and various characteristics of B-cell spatial patterns, as well as Fan classification.

The formalin-fixed and paraffin-embedded diagnostic lymph node samples of 53 children and adolescents with stage IA or IIA NLPHL who had been enrolled in the EuroNet-PHL-LP1 trial were analyzed. All patients were treated with 3 cycles of CVP chemotherapy (cyclophosphamide 500 mg/m^2 intravenously on day 1, vinblastine 6 mg/m^2 intravenously on days 1 and 8, and prednisolone 40 mg/m^2 orally on days 1-8). The interval between chemotherapy cycles was scheduled for 1 or a maximum of 2 weeks. At the end of chemotherapy, response assessment was performed using positron emission tomography combined with contrast-enhanced computed tomography (PET-CT). The response was

Submitted 8 May 2023; accepted 15 August 2023; prepublished online on *Blood Advances* First Edition 23 August 2023; final version published online 13 October 2023. https://doi.org/10.1182/bloodadvances.2023010652.

*S.S. and A. Shankar are joint first authors.

†C.M-K., D.K., and S.G. are joint last authors.

Data will be available upon reasonable request from the corresponding author, Stefan Gattenloehner (Stefan.Gattenloehner@patho.med.uni-giessen.de).

The full-text version of this article contains a data supplement.

Table 1. LP and B-cell spatial variables and Fan pattern according to treatment response

	good	poor	*P*/alpha'/*r*
Patients (total)	33	20	NA
Females (typical pattern)	4	5	NA
Females (variant pattern)	4	2	NA
Males (typical pattern)	19	5	NA
Males (variant pattern)	6	8	NA
Fan classes (variant / typical)	10 / 23	10 / 10	0.24
Age, y	11.4 (3.6-17.9)	13.45 (4.9-17.6)	0.61
menclus, cells/cluster	**161.5 (64.5)**	**87.5 (56)**	**0.0012/0.008*/0.45**
tumorD, cells/mm^2	**61.3 (32.4)**	**40.6 (23.2)**	**0.0049/0.01*/0.39**
madclus, cells/cluster	**60.8 (19.8)**	**46.7 (16.5)**	**0.017/0.0125**
LPm3, μm	**74.4 (22.8)**	**85 (17.6)**	**0.071/0.017**
LPmad3, μm	**38.5 (14.6)**	**45 (15.2)**	**0.14/0.025**
Nuclear area, μm^2	**117.4 (14.1)**	**124.2 (21.5)**	**0.27/0.05**
bcellD, cells/mm^2	3756.2 (2157.8)	2803 (1594.3)	0.14
MdistB, μm	6.4 (0.5)	6.5 (0.4)	0.23
McrossLPb, μm	12.5 (2.7)	13.1 (3.3)	0.4
otherD, cells/mm^2	10 973.6 (2 192.2)	11 151 (2989.8)	0.79

Results are presented as the median (MAD), except for age, which is presented as the median (min-max). *P* is Fisher exact test *P* value (Fan) or Mann-Whitney *U* test *P* value (other variables), alpha' is the local significance level, adjusted using the Bonferroni-Holm method to attain a target level of 0.05, for 6 focal variables (indicated in bold). The Wilcoxon effect size *r* was calculated for significance tests.

*Indicate significant differences between the groups.

categorized as "good" if the PET was negative and at least a 75% reduction of the initial tumor mass across all initially affected lymph nodes was achieved. "Poor" response was characterized by PET positivity and/or a volume reduction of less than 75% compared with the initial tumor mass in at least 1 initially involved lymph node region (Table 1). The pathological features were categorized according to the Fan classification into typical NLPHL (patterns A and B) and variant patterns (patterns C-F) (Table 2).

OCT2 immunostained slides of the samples (ZS02 antibody; Zytomed Systems, Berlin, Germany) were digitized using Pannoramic SCAN II (3DHISTECH, Budapest, Hungary) and the resulting digital slides were divided into 256 × 256 pixel tiles using QuPath.[12] To capture variability, 14579 LP cells, 157236 B cells, and 379114 other cells were semimanually annotated using LabelImg[13] in a subset of 9153 tiles from 35 study cases and 70 NLPHL cases outside the study. Using transfer learning, a pretrained YOLOv4-tiny convolutional neural network[14] was retrained on these tiles. The retrained network was then used to detect cells across all tiles. The centers of the frames or bounding boxes around the detected cells ("cell centroids") were then converted into marked planar point patterns representing the tissue using the R package spatstat version 2.1[15] and a custom R script.

Table 2. Stratification of the study cohort based on Fan et al, 2003

Fan patterns			Frequency	Response	Proportion of poor
	Primary	Secondary		poor/good	responders
Typical[b]			**33**	**10/23**	**0.3**
	A	No	30	9/21	
	A	B	3	1/2	
Variant[b]			**20**	**10/10**	**0.5**
	A	C	5	4/1	
	C	No	9	3/6	
	C	E	1	1/0	
	E	C	3	1/2	
	E	No	2	1/1	

b Rows with the bold text/numbers indicate summarized rows below

To characterize each LP point pattern, we selected 6 spatial variables based on published literature (Figure 1).[11,16,17] These variables included the nuclear area approximated from the median area of the detected LP cell bounding boxes, LP cell density (tumorD) calculated by dividing the number of LP cell centroids by the tissue area, the median Euclidean distance between LP points and their third nearest neighbors of the same type (LPm3), as well as LPmad3, its median absolute deviation (MAD), and the median (menclus) and MAD (madclus) of the number of cells in putative clusters of LP cells detected by affinity-propagation clustering (apcluster version 1.4.9[18]), a data-driven approach to group data points without the need to predefine the number of clusters.[19] As a confirmatory analysis, Mann-Whitney *U* tests were used to analyze the potential association between these spatial variables and treatment response, with local significance levels adjusted using the Bonferroni-Holm step-down procedure to maintain an overall significance level of 0.05. To gain further insight, we measured the density of B cells (bcellD) and other cells (otherD) and the median nearest-neighbor distances between B cells (MdistB) and between LP and B cells (McrossLPb). We then performed exploratory

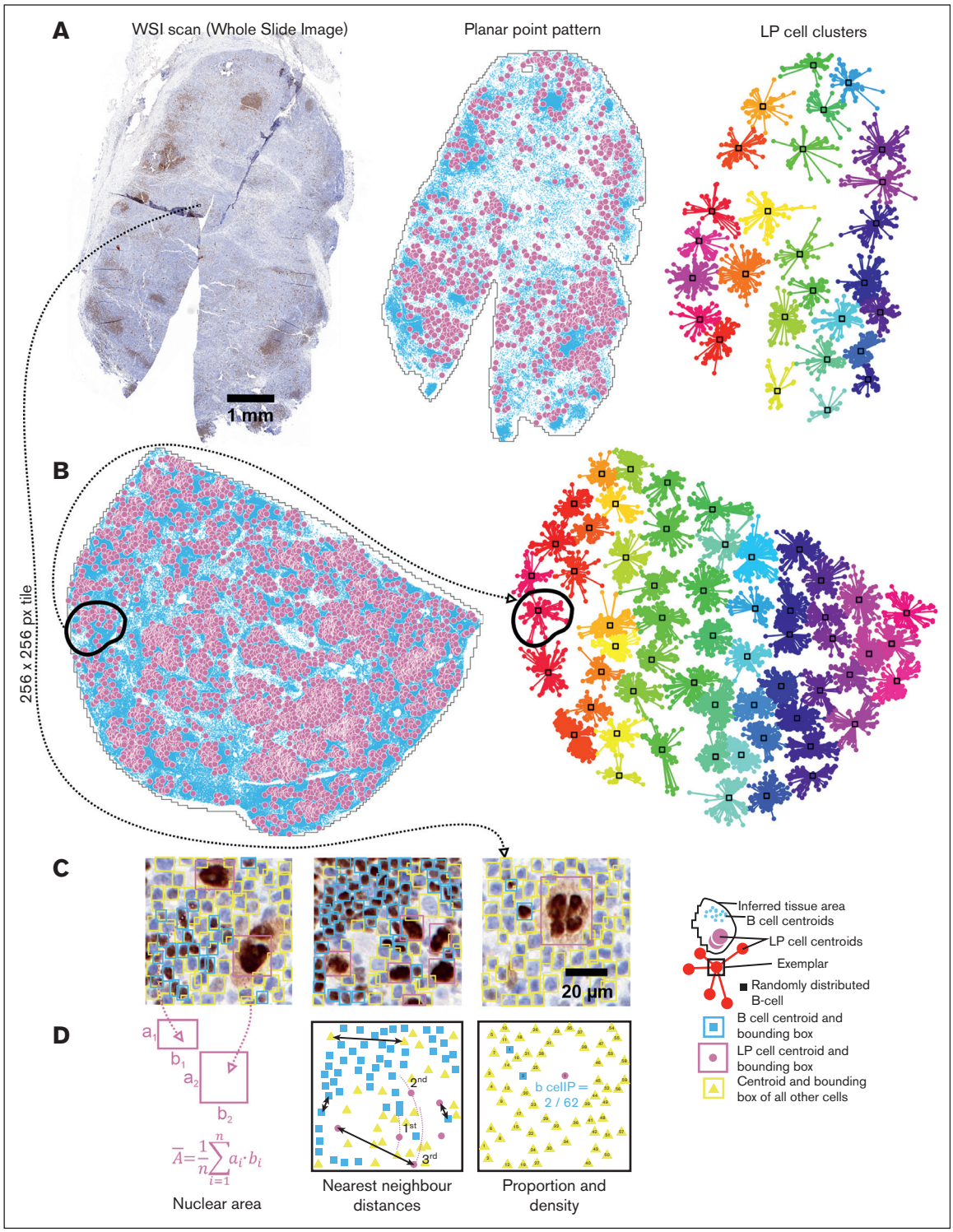

Figure 1. Spatial variable extraction from digital slides using deep-learning, affinity-propagation clustering, and spatial statistics. (A) Left to right: Whole-slide image scan of an OCT2-stained tissue section of NLPHL with Fan pattern "C." A highlighted 256 × 256-pixel tile is magnified in panel C. The planar point pattern after cell detection, showing LP cell and B-cell centroids. LP cell clusters are identified using affinity-propagation clustering. (B) Planar point pattern and result of affinity-propagation clustering of LP cell centroids in an NLPHL case with Fan pattern "A." A specific cluster is highlighted in both the point pattern and cluster plot. (C) Individual tiles with detected cells enclosed within bounding boxes. The deep-learning detection precision was 95.43%. (D) Point patterns of the tiles with symbols indicating different cell types and spatial variables, including the area of bounding boxes as an approximation of the nuclear area, nearest neighbor distances between cell centroids, and point counts for cell density calculation.

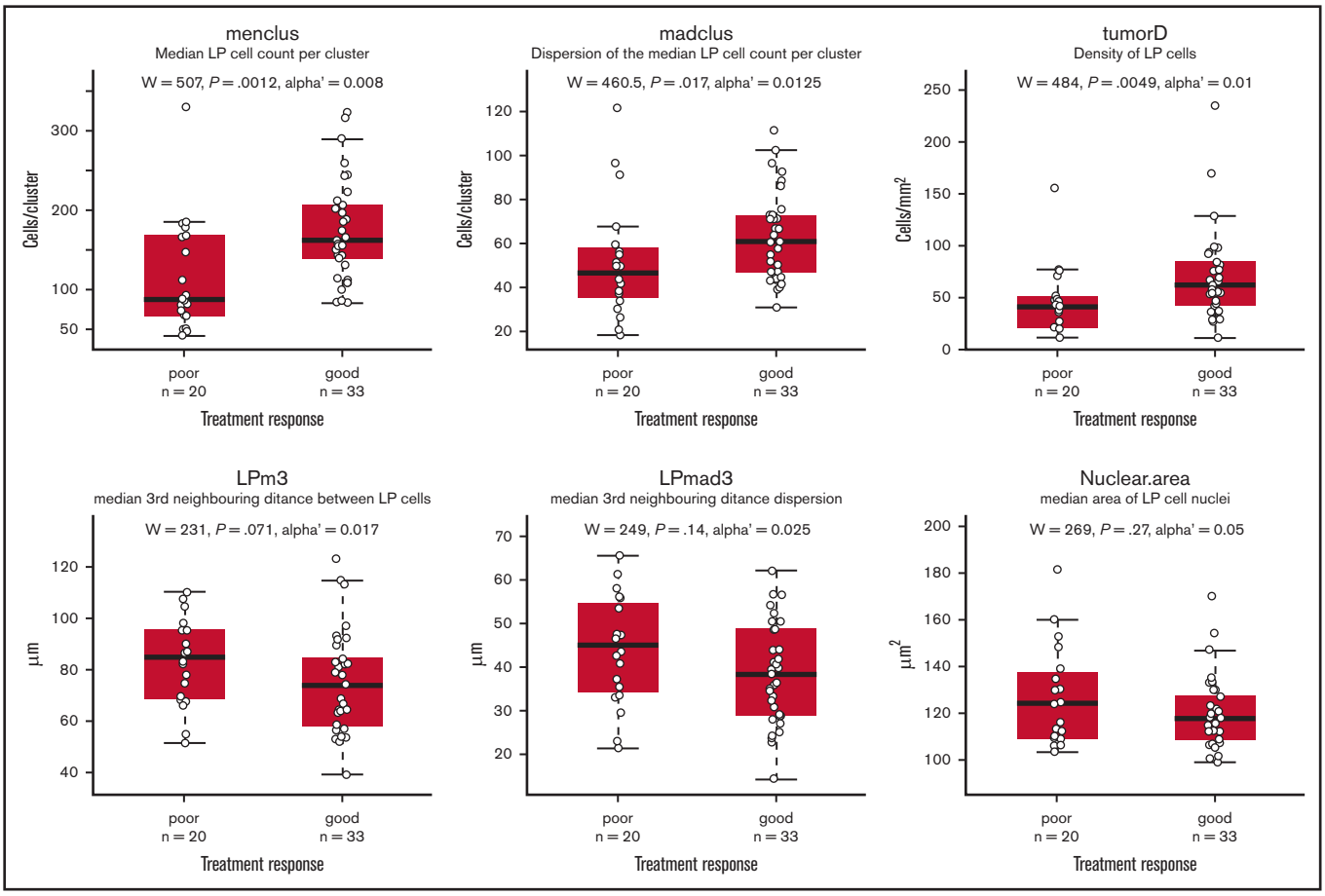

Figure 2. Comparison of LP cell-derived spatial variables grouped by treatment response in patients with NLPHL. The Mann-Whitney *U* test was used to compare treatment response groups, with the *P* value and Holm-Bonferroni adjusted local significance level (alpha') for a target alpha of 0.05, as shown above the plot. The results indicate that the density and number of LP cells per cluster were significantly different between the treatment response groups. The plot shows individual data points as empty circles, with the median depicted as a black bar, the upper and lower quartiles shown in a red box, and whiskers representing 1.5 times the interquartile range. A small value of n refers to the number of cases per group.

Mann-Whitney *U* tests for B-cell spatial variables against response. Similarly, we used Fisher exact test to examine the proportion of bad responders with typical and variant Fan patterns. Notably, multiple testing correction was not applied in any of the analyses. All analyses were conducted using R version 4.1.0.[20]

Deep learning achieved a high mean average precision in cell detection, comparable with that reported in the literature[21] (mean ± SD: 95.24 ± 0.17%). In patients with poor response, the number of LP cells per cluster was nearly half that of those with good response (median ± MAD: 87.5 ± 56 vs 161.5 ± 64.5; P = .0012; Table 1, Figure 2). Correspondingly, the density of LP cells was 1.5 times lower in poorly responding patients compared with those with good response (median ± MAD: 40.6 ± 23.2 cells/mm^2 vs 61.3 ± 32.4 cells/mm^2; P = .0049; Table 1, Figure 2). These findings were statistically significant after adjustment for multiple tests. It is counterintuitive that a poor chemotherapy response was associated with a lower LP cell density. However, LP cell density was measured before treatment; thus, differences in LP cell proliferation or apoptosis rates may explain the relationship between poor chemotherapy responses and lower LP cell density.[22,23] For example, slow-cycling drug-tolerant cancer cells are known to contribute to therapy failure in lymphoma and other cancer types.[24,25] However, preliminary analysis could not confirm the hypothesis (refer to supplemental Information for details). Although LP cell size was previously hypothesized to hinder tumor spread,[11] we found no difference in LP cell nuclei size between Fan patterns or good and poor responders. Additional studies are required to investigate LP cell density differences, their association with chemotherapy failure in pediatric NLPHL, and their potential as a prognostic marker in this context.

Our exploratory analysis found no correlation between Fan classification or B-cell pattern variables and treatment response (Tables 1 and 2). In 10 out of 33 good responders, variant Fan patterns were found, compared with 10 variant patterns out of 20 poor responders (P = .24, Fisher exact test). This indicates that Fan classification is not useful for risk stratification in pediatric patients with early-stage NLPHL.

The limitations of this investigation are the small cohort size and the exclusive use of CVP therapy. Our findings may not apply to advanced-stage pediatric patients or adults.

In summary, LP cell distribution was significantly correlated with early chemotherapy response. To our knowledge, our report is the first to show a significant correlation between early chemotherapy response and cancer cell spatial pattern characteristics in pediatric NLPHL and might be useful for future risk-adapted trials.

Acknowledgments: The authors kindly thank Deutsche Krebshilfe, Elternverein für Leukämie- und krebskranke Kinder, Giessen e.V., Menschen für Kinder e.V., Tour der Hoffnung e.V., and Kinderkrebshilfe of the Journal Oldtimer Markt Mainz for their generous financial support. The authors also thank Sylvia Hartmann for reviewing the immunoarchitectural patterns of samples from Germany. A.B., D.K., C.M-K., and S.G. were supported by Deutsche Krebshilfe through grant DKH-70114098. C.M-K. and D.K. were supported by the Deutsche Krebshilfe grant DKH-108661.

Contribution: A.B., D.K., and S.G. conceptualized the research and obtained funding; A. Shankar reviewed the UK samples; C.M-K. reviewed samples from Germany; L.W. trained the neural network; S.S. developed the workflow and reconstructed and analyzed point patterns; S.S., D.H., and A. Schneider performed statistical analyses; and all authors contributed to the concept, drafting of the manuscript, and critically reviewed, edited, and approved the final manuscript.

Conflict-of-interest disclosure: The authors declare no competing financial interests.

ORCID profile: S.S., 0000-0003-3212-8722.

Correspondence: Stefan Gattenloehner, Department of Pathology, University Hospital Giessen and Marburg GmbH, Langhansstrasse 10, 35392, Giessen, Germany; email: Stefan.Gattenloehner@patho.med.uni-giessen.de.

References

1. Alaggio R, Amador C, Anagnostopoulos I, et al. The 5th edition of the World Health Organization classification of haematolymphoid tumours: lymphoid neoplasms. *Leukemia*. 2022;36(7):1720-1748.
2. Campo E, Jaffe ES, Cook JR, et al. The International Consensus Classification of Mature Lymphoid Neoplasms: a report from the Clinical Advisory Committee. *Blood*. 2022;140(11):1229-1253.
3. Eichenauer DA, Engert A. Nodular lymphocyte-predominant Hodgkin lymphoma: a unique disease deserving unique management. *Hematology Am Soc Hematol Educ Program*. 2017;2017(1):324-328.
4. Eichenauer DA, Plütschow A, Fuchs M, et al. Long-term follow-up of patients with nodular lymphocyte-predominant Hodgkin lymphoma treated in the HD7 to HD15 trials: a report from the German Hodgkin Study Group. *J Clin Orthod*. 2020;38(7):698-705.
5. Hodgson DC. Late effects in the era of modern therapy for Hodgkin Lymphoma. *Hematology*. 2011;2011(1):323-329.
6. Mauz-Körholz C, Lange T, Hasenclever D, et al. Pediatric nodular lymphocyte-predominant Hodgkin lymphoma: treatment recommendations of the GPOH-HD Study Group. *Klin Padiatr*. Published online 10 September 2015. https://doi.org/10.1055/s-0035-1559664
7. Fan Z, Natkunam Y, Bair E, Tibshirani R, Warnke RA. Characterization of variant patterns of nodular lymphocyte predominant Hodgkin lymphoma with immunohistologic and clinical correlation. *Am J Surg Pathol*. 2003;27(10):1346-1356.
8. Shankar AG, Kirkwood AA, Hall GW, Hayward J, O'Hare P, Ramsay AD. Childhood and Adolescent nodular lymphocyte predominant Hodgkin lymphoma–a review of clinical outcome based on the histological variants. *Br J Haematol*. 2015;171(2):254-262.
9. Hartmann S, Eichenauer DA, Plütschow A, et al. The prognostic impact of variant histology in nodular lymphocyte-predominant Hodgkin lymphoma: a report from the German Hodgkin Study Group (GHSG). *Blood*. 2013;122(26):4246-4252. quiz 4292.
10. Untanu RV, Back J, Appel B, et al. Variant histology, IgD and CD30 expression in low-risk pediatric nodular lymphocyte predominant Hodgkin lymphoma: a report from the Children's Oncology Group. *Pediatr Blood Cancer*. 2018;65(1):e26753.
11. Hartmann S, Soltani AS, Bankov K, et al. Tumour cell characteristics and microenvironment composition correspond to clinical presentation in newly diagnosed nodular lymphocyte-predominant Hodgkin lymphoma. *Br J Haematol*. 2022;199(3):382-391.
12. Bankhead P, Loughrey MB, Fernández JA, et al. QuPath: Open source software for digital pathology image analysis. *Sci Rep*. 2017;7(1):16878.
13. Tzutalin. LabelImg. Published online 2015. Accessed 23 June 2022. https://github.com/tzutalin/labelImg
14. Bochkovskiy A, Wang CY, Liao HYM. YOLOv4: optimal speed and accuracy of object detection. *arXiv*. Preprint posted online 23 April 2020. http://arxiv.org/abs/2004.10934
15. Baddeley A, Turner R. spatstat: an R package for analyzing spatial point patterns. *J Stat Softw*. 2005;12(6):1-42.
16. Chakiryan NH, Kimmel GJ, Kim Y, et al. Spatial clustering of CD68+ tumor associated macrophages with tumor cells is associated with worse overall survival in metastatic clear cell renal cell carcinoma. *PLoS One*. 2021;16(4):e0245415.
17. Parra ER. Methods to determine and analyze the cellular spatial distribution extracted from multiplex immunofluorescence data to understand the tumor microenvironment. *Front Mol Biosci*. 2021;8:668340.
18. Bodenhofer U, Kothmeier A, Hochreiter S. APCluster: an R package for affinity propagation clustering. *Bioinformatics*. 2011;27(17):2463-2464.
19. Frey BJ, Dueck D. Clustering by passing messages between data points. *Science*. 2007;315(5814):972-976.
20. R Core Team. *R: A Language and Environment for Statistical Computing*. Accessed 30 June 2021. http://www.r-project.org
21. Wang CW, Huang SC, Lee YC, Shen YJ, Meng SI, Gaol JL. Deep learning for bone marrow cell detection and classification on whole-slide images. *Med Image Anal*. 2022;75:102270.
22. Remvikos Y, Beuzeboc P, Zajdela A, Voillemot N, Magdelénat H, Pouillart P. Correlation of pretreatment proliferative activity of breast cancer with the response to cytotoxic chemotherapy. *J Natl Cancer Inst*. 1989;81(18):1383-1387.
23. Dinand V, Malik A, Unni R, Arya LS, Pandey Rm, Dawar R. Proliferative index and CD15 expression in pediatric classical Hodgkin lymphoma. *Pediatr Blood Cancer*. 2008;50(2):280-283.
24. Klener P, Klanova M. Drug resistance in non-Hodgkin lymphomas. *Int J Mol Sci*. 2020;21(6):2081.
25. Shen S, Vagner S, Robert C. Persistent cancer cells: the deadly survivors. *Cell*. 2020;183(4):860-874.